Available online at www.sciencedirect.com

ScienceDirect

Procedia Materials Science 8 (2015) 1140 – 1149

Procedia Materials Science

www.elsevier.com/locate/procedia

International Congress of Science and Technology of Metallurgy and Materials, SAM - CONAMET 2013

Microstructural study of welded joints in a high temperature martensitic-ferritic ASTM A335 P91 steel

Nilthon Zavaleta Gutiérrez[a], Jorge Vera Alvarado[a], Hernán de Cicco[b], Ariel Danón[b]*

[a]*Departamento de Minas y Metalurgia, Facultad de Ingeniería, Universidad Nacional de Trujillo, Av. Juan Pablo II s/n, Trujillo, Perú*
[b]*Gerencia Materiales, Comisión Nacional de Energía Atómica, Av. Gral Paz 1499 B1650KNA, San Martín, Buenos Aires, Argentina*

Abstract

We have studied the effect of post-weld heat treatments (PWHT's) performed at 760 ºC on the microstructure and hardness of ASTM A335 P91 steel welded joints. The welding process used was GMAW and the filler material was a solid wire of the type AWS ER90S-B9. The analysis of cross sections of the welds revealed a narrow heat-affected zone (HAZ) 4 mm wide, composed by a thin (~0.2 mm) coarse-grained layer with high hardness, a fine-grained region exhibiting grains up to 4 μm in size, and a soft intercritical region with low hardness, located 3 to 4 mm away from the fusion line. The results of hardness measurements suggest that a PWHT of 2h at 760 ºC is enough to reestablish the strength of the P91 steel after the welding process.

Selection and peer-review under responsibility of the scientific committee of SAM - CONAMET 2013

Keywords: Martensitic-ferritic steel, hardness, welding, post-weld heat treatment

1. Introduction

Martensitic-ferritic steels of the P91/T91 type have been widely used in applications to structural components foreseen for working at high temperature (up to 600 ºC), and requiring for this reason an exigent combination of properties such as oxidation resistance and high creep strength. Both steels contain approximately 9%Cr, 1%Mo and minor amounts of Nb, V and N; their properties and applications have already been extensively reviewed, see for instance Orr and Burton (1992) or Foldyna et al. (1996).

* Corresponding author. Tel.: 005411-6772-7264; fax: 005411-6772-7362
E-mail address: danon@cnea.gov.ar

Selection and peer-review under responsibility of the scientific committee of SAM - CONAMET 2013
doi:10.1016/j.mspro.2015.04.178

One of the most common problems encountered in using these steels is the reduction in the creep strength of welded joints, especially in the range of low stresses and long exposures. The joints tend to fail in the intercritical and fine-grained regions of the heat-affected zone (ICHAZ and FGHAZ), characterized for peak temperatures located, respectively, between A_{c1} and A_{c3} and slightly above A_{c3}. The failure is known as Type IV crack, and the mechanism for it to occur is not fully understood yet (Bell (1997), Ellis and Viswanathan (1998), Hasegawa et al. (2001), Francis et al. (2006)). Despite this lack of full explanation, it is generally assumed that microstructural changes occurring during the welding and PWHT processes will affect the creep resistance of the welded joint.

Hardness –a macroscopic "probe" commonly used to detect microstructural changes- has been shown to diminish in the ICHAZ after post weld heat treatment (PWHT). However, after Francis et al. (2006), the relationship between hardness and Type IV failure susceptibility is not straightforward: at high stresses, the minimum creep strength microstructure coincides with the minimum hardness microstructure –i.e., the ICHAZ- but at low stresses, typical of service conditions, the creep life is a minimum in the FGHAZ, which does not have the minimum hardness.

The aim of this paper is to report on the first step of a research on the relationship between welding conditions and further creep strength of a P91 steel, by studying the influence of PWHT's carried out at 760 ºC on the hardness profile and the microstructure of multipass welded joints.

Nomenclature

GMAW	Gas Metal Arc Welding
AW	As-Welded (sample)
HAZ	Heat Affected Zone
ICHAZ	Intercritical Heat Affected Zone
CGHAZ	Coarse Grained Heat Affected Zone
FGHAZ	Fine Grained Heat Affected Zone
PWHT	Post Weld Heat Treatment
FEGSEM	Field Emission Gun Scanning Electron Microscope

2. Experimental procedure

The base material was taken from a seamless pipe of ASTM A335 P91 steel provided by Dalmine Tenaris (Italy). The dimensions of the pipe were 219.1 mm outer diameter and 31.75 mm wall thickness. The filler material was a solid wire 1.2 mm in diameter according to the norm AWS ER90S-B9. The chemical compositions of the base material and filler material are shown in Table 1.

Table 1. Chemical composition of the base material ASTM 335 P91 and filler material (wt. %)

Material	C	Si	Mn	P	S	Cr	Mo	Ni	Nb	V	N
ASTM 335 – P91	0.10	0.24	0.36	0.014	0.01	8.37	0.88	0.15	0.075	0.211	0.0605
AWS ER90S-B9	0.07-0.13	1.50-0.30	1.25	0.01	0.01	8.0-9.5	0.8-1.10	1.0		0.15-0.25	

The joints to be welded were machined according to the norm ASME B31.3, Figs. 1 (a) and (b). After machining, the joint pieces were cut so as to obtain circular sectors defined by a 120º angle that were used to produce the welds (Figs. 1 (c) and (d)). Welding was done using the GMAW process. The welding conditions are shown in Table 2 along with the multipass sequence. According to these conditions, the heat input was calculated as approximately 1.2 kJ/mm. Once the joint was welded, a cross section was cut in order to characterize the microstructure of the as-welded material. The rest of the as-welded joint was then cut in four pieces, each of which was submitted to PWHT's of 1, 2, 4 and 8 h. respectively. Four more cross-sections were obtained from the material in each of the as-treated conditions. Characterization of the cross-sections was done by optical microscopy -using a Leica DMILM microscope attached with a Canon Power Shot S80 camera- and scanning electron microscopy, using a Carl Zeiss Supra 40 FEG-SEM. Etching was accomplished using the standard Villela reagent for SEM observations and

electrolytically by using a 10 % oxalic acid reagent at 6 V for optical microscopy, the last procedure allowing for a better visualization of the prior austenite grain boundaries.

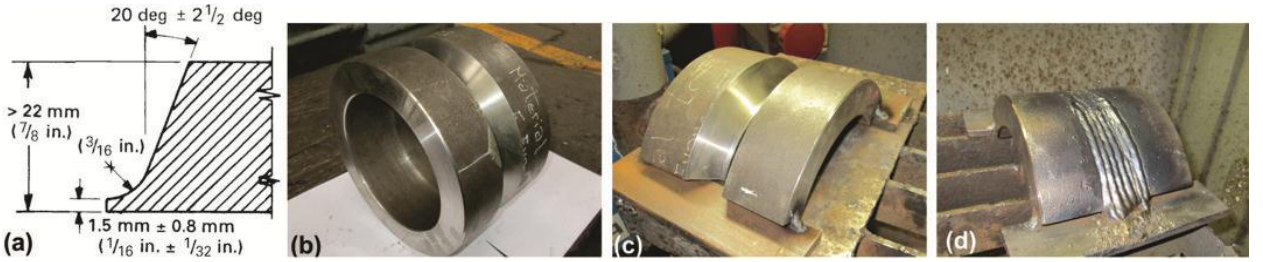

Fig. 1. (a) Geometry of the joint according to ASME B31.3; (b) Pipe machined according to (a); (c) Joint pieces cut at 120 º and ready to be welded; (d) welded joint.

Hardness measurements were done by means of an Indentec digital durometer, using 5 kf preload and a diamond Vickers indenter. Before measurements, the cross sections were etched with the Villela reagent for 2 min. to make the weld macroscopically visible.

Table 2. Welding parameters and welding process features

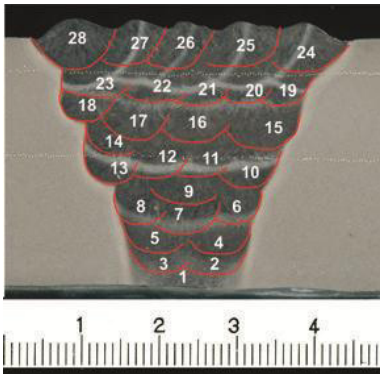

Welding process features	
Type	GMAW
Filler	AWS ER90S-B9
Protection Gas	98% Ar + 2% CO_2
Flow	20 l/min
Welding Parameters	
Pre-Heating Temperature (ºC)	200 - 260
Current Intensity (A)	160-180
Voltage (V)	22 – 26
Polarity	DCEP
PWHT Temperature (ºC)	760

Measurements were performed along two lines located at 5 and 16 mm from the weld surface, crossing the whole weld bed (see Table 2). Finally, X-ray diffraction spectra were taken from the central part of the weld bed region for the samples as-welded and post-weld-treated for 2 and 8 hours. Measurements were done in the Bragg-Brentano geometry within the angular interval between 35 and 120 º using Ni-filtered CuKα radiation and a graphite plane monochromator. The diffracted radiation was collected with a PixCel 3D ultrafast detector, which allowed a good counting statistics in a non time-consuming schedule. The experimental XRD patterns were refined by the Rietveld method using the software Maud (Materials Analysis Using Diffraction) developed by Lutterotti et al.(1999); a pattern of pure Si standard material obtained in the same experimental conditions was also refined so as to get the parameters of the instrumental function.

3. Results and discussion

3.1 Microstructure and hardness of the as-welded P91 steel

The microstructural features in the different regions of the weld bed are shown in Fig. 2. The weld metal has a structure of columnar grains that follow the thermal gradient imposed during the welding procedure. During cooling, the final transformation is the martensitc one, which could convey an autotempering process to some extent.

Autotempering would be unavoidable due to the low carbon content –and hence high M_s- of the steel (Aborn (1956)); the small, rod-like precipitates seen in the bulk of martensite laths would be M_3C particles (M=Fe,Cr) formed during this process, Fig. 2(b).

In the CGHAZ, austenite reaches high peak temperature values after full austenite transformation, these temperature values promoting an almost complete dissolution of the precipitates inherited from the as-received state and hence allowing for significant grain growth; the measured width of the CGHAZ was ~ 200 μm. The high temperature values are reached only in a narrow region away from the fusion line; this is probably due to a pronounced thermal gradient imposed from the weld metal to the base metal and coming from a reduced thermal conductivity of high-Cr steels as compared, for instance, with low carbon structural steels (Grong (1994)).

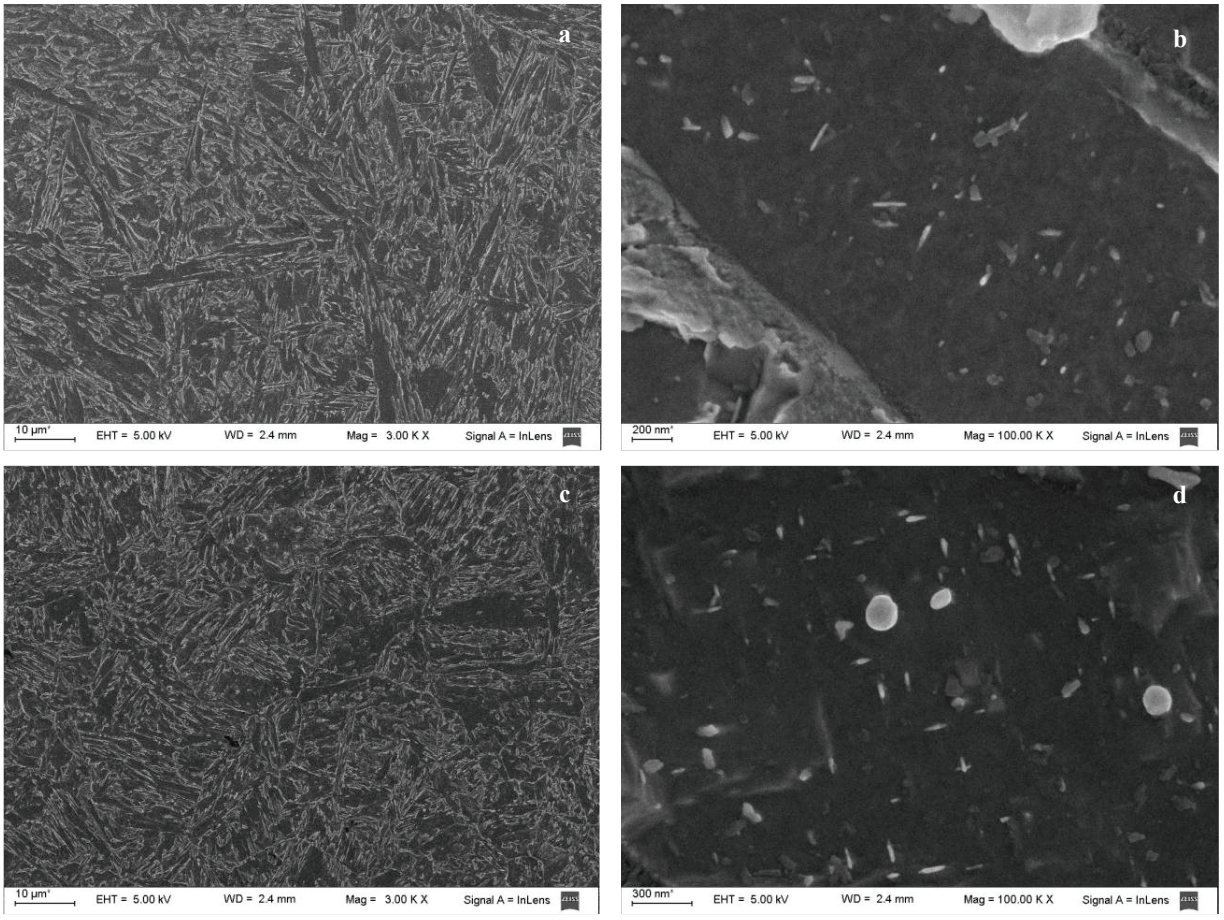

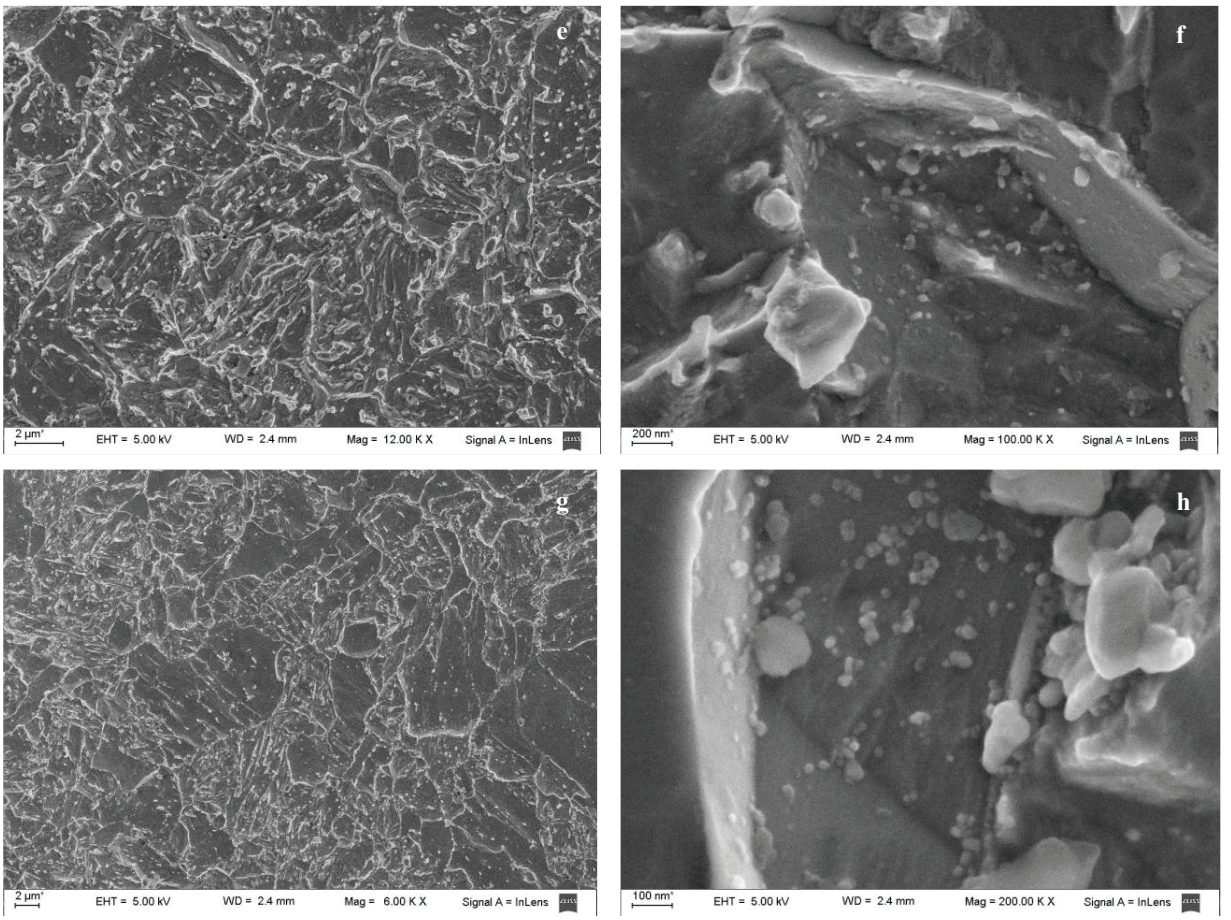

Fig 2. FEG-SEM micrographs of the P91 steel in the as-welded condition. (a) and (b) weld metal; (c) and (d) CGHAZ; (e) and (f) FGHAZ; (g) and (h) ICHAZ.

In the same way as for the weld metal, the small, strongly oriented precipitates formed in the interior of martensite laths of the CGHAZ during cooling (Fig. 2 (d)) would be M_3C. A few spherical precipitates –probably of the Nb-rich MX type- are also observed in this region. These coarse MX precipitates would remain undissolved during the complete thermal cycle due to their low solubility product (Tamura et al. (2001)).

Fig. 3 shows the hardness profile across the weld metal, reflecting (especially the profile obtained at 16 mm from the bed surface) the microstructural variations occurring during the multipass welding process. Such variations could correspond to the formation of the columnar grained, coarse grained and fine grained recrystallized regions.

During welding, transformation to austenite in the FGHAZ is complete, but the peak temperature reaches a value only slightly above A_{c3}; thus, the carbide particles inherited from the initial state are hardly dissolved and contribute to keep fine the austenite grain size, i.e. 3 to 4 µm (Fig. 2(e)). At the same time, as a large fraction of carbon remains bound to undissolved carbides, autotempering would be severely reduced, and in fact the small, oriented rod-like precipitates are hardly detected (Fig. 2 (f)). This region of the HAZ is the widest one.

On the other hand, the ICHAZ is characterized by a peak temperature located between A_{c1} and A_{c3} and hence by a partial transformation to austenite. This means the coexistence of transformed and non-transformed regions, i.e. small prior austenite grains transformed to fresh martensite and large regions of overtempered, non transformed martensite respectively (Figs. 2 (g) and (h)). In these last regions, microscopic observations suggest that precipitates

have coarsened and lowered their number density with respect to transformed regions. The same observation has already been reported in the previous literature (Moitra et al. (2002)).

3.2 Microstructure and hardness of the P91 steel after PWHT

The microstructural heterogeneity across the weld bed increases by submitting samples to a PWHT. The weld metal keeps its columnar morphology, but its hardness drops as the time of PWHT increases (see Figs. 4 and 5). This hardness drop is due to the recovery of the martensite matrix and the coarsening of precipitates. The results obtained for the average hardness of the weld metal at different PWHT times (Fig. 5(a)) indicate that 2h tempering at 760 ºC is enough to reestablish a hardness value close to that of the base metal; longer PWHT times will produce only further diminutions of the hardness value and likely, of the strength of the weld.

In the CGHAZ, precipitate dissolution makes alloying elements go into solid solution during the welding process; these elements will re-precipitate during PWHT and this would explain the hardness peak observed close to the fusion line in all the treated samples (Figs. 4 and 5 (b)). The hardness peak diminishes its value for longer PWHT times; this could be again associated to the recovery of martensite and the coarsening of $M_{23}C_6$ precipitates (Zavaleta Gutiérrez et al. (2010)).

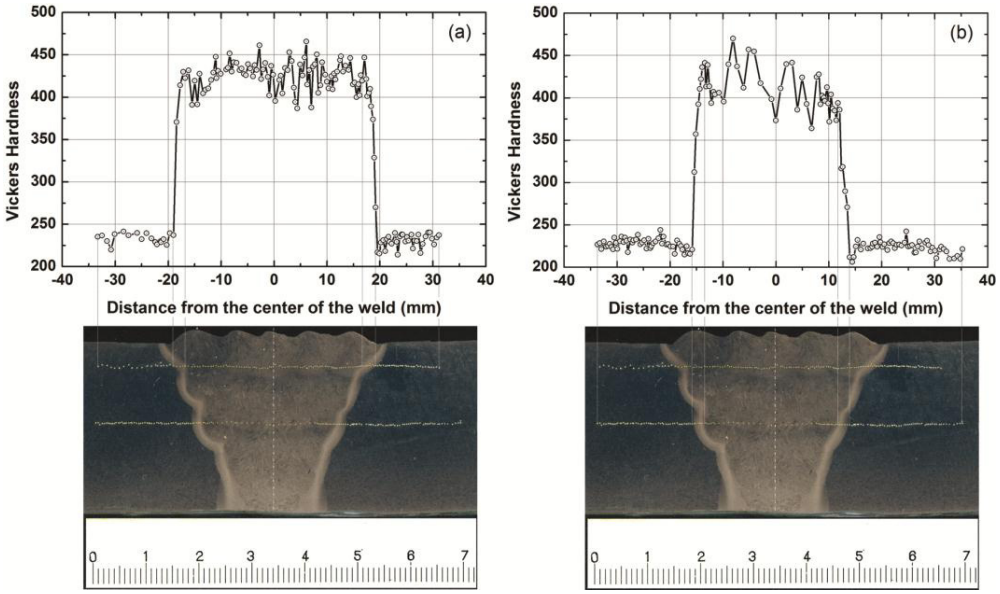

Fig. 3. Hardness profile measured at distances of 5 mm (a) and 16 mm (b) from the weld surface across the weld metal of the as-welded P91 steel.

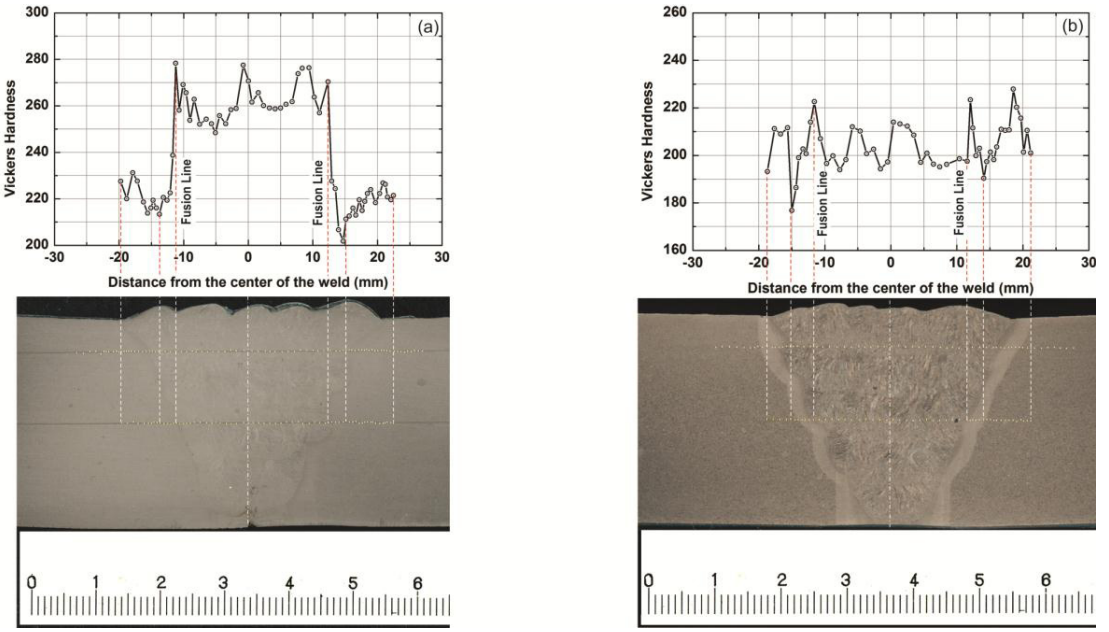

Fig. 4. Hardness profile measured across the weld metal at 16 mm from the weld surface of the P91 steel PWH treated for 1 h (a) and 8h (b) at 760 ºC.

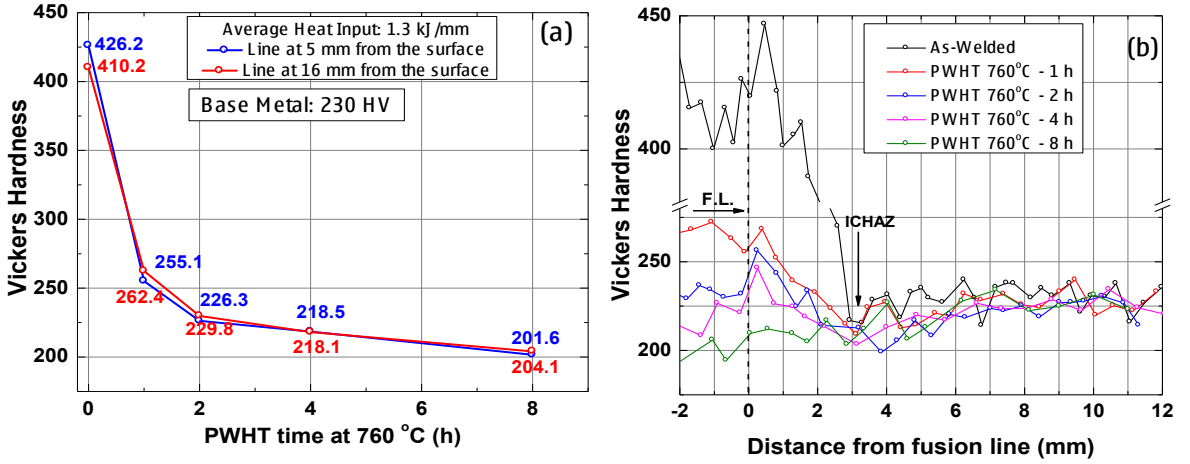

Fig. 5. Variation of the average hardness of the weld metal (a) and hardness across the welded joint (b) of the P91 steel for increasing PWHT time.

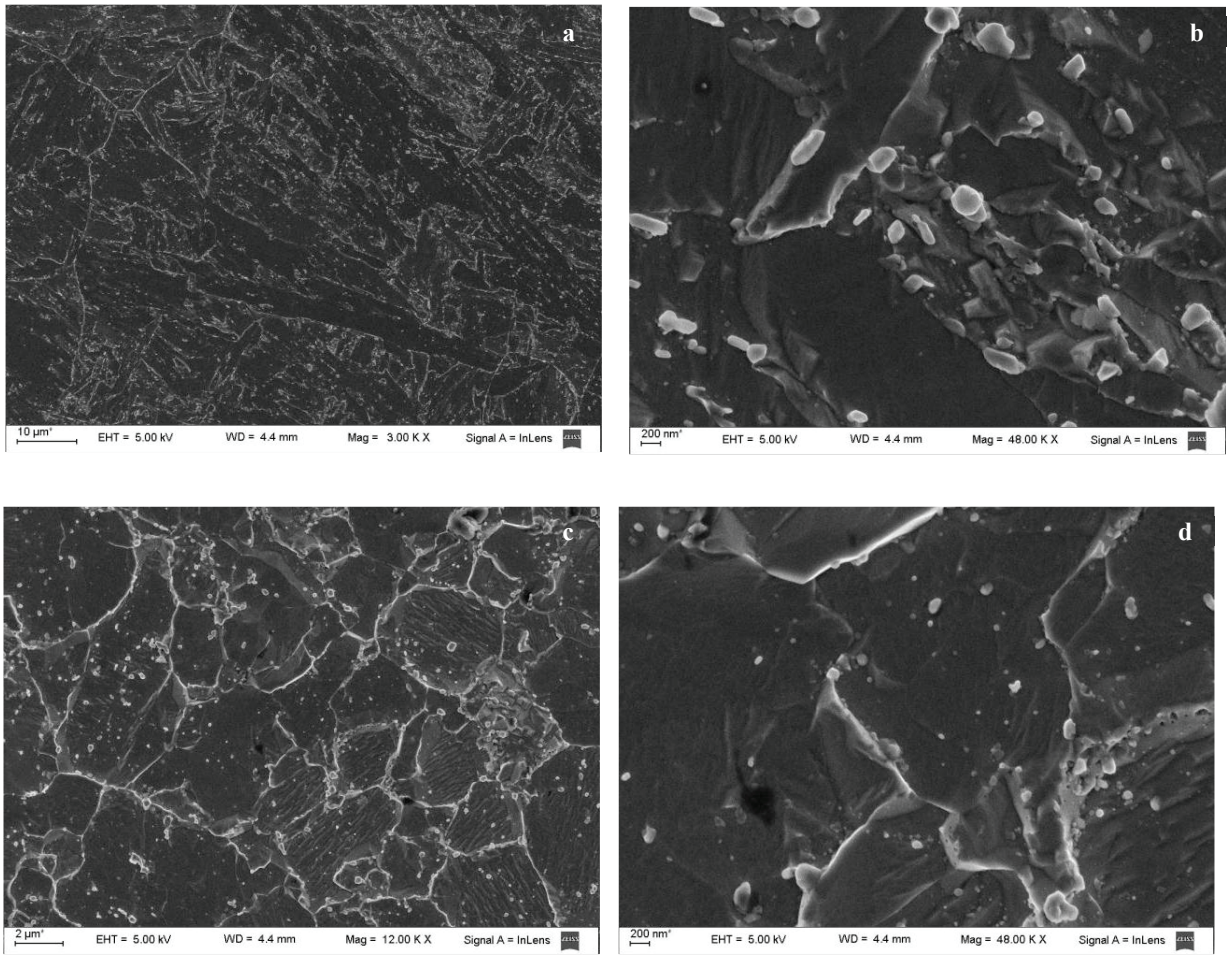

Fig. 6. FEG-SEM micrographs of the P91 steel as-treated for 2h at 760 ºC, CGHAZ (a) and (b), FGHAZ (c) and (d).

The FGHAZ is the widest among the HAZ regions; the estimated prior austenite grain size in this region amounts approximately 3- 4 µm and its hardness after PWHT is lower than the one measured in the CGHAZ (Fig. 5(b)). The hardness drop in the FGHAZ after PWHT could be explained on the basis of an increased recovery of the martensite matrix. A higher degree of recovery in the FGHAZ would be possible because the fraction of precipitates dissolved in it during the welding cycle is significantly lower than the fraction dissolved in the CGHAZ; these non-dissolved precipitates coarsen during PWHT and lose their ability to pin martensite interfaces. On the opposite, fine precipitates would nucleate in the CGHAZ during PWHT due to the high solute content inherited from austenite; these fine precipitates would have a more appropriate size and a more uniform distribution to stabilize the martensitic structure.

The ICHAZ is characterized by a pronounced microstructural heterogeneity, arising from the coexistence of transformed and non-transformed portions of the matrix. This heterogeneity could be on the basis of the measured diminution of the hardness, which reaches a minimum value approximately at 3 to 4 mm from the fusion line within this region (Fig. 5 (b)). On the other hand, this zone has been identified as the one more prone to fail by Type IV cracking (Viswanathan (1989), Bell (1997)).

The previous discussion suggests that, other parameters being fixed, the time of treatment could provide a key to control the microstructural changes that occur during PWHT, in order to minimize the effects of these changes on the creep strength.

3.3 X-ray diffraction

Fig. 7 shows magnified views of the diffractograms obtained for the AW and PWHT (8h) samples. In the first case, (Fig 7(a)) retained austenite has been unambiguously identified. At the same time, two martensite phases were assumed for Rietveld modeling, in order to take into account the probable mixing of fresh martensite regions with overheated martensite regions during the different passes. With this two-martensite model the refinement turned out to improve significantly. In the case of the XRD spectrum of the PWH treated sample (Fig. 7(b)), the presence of the precipitated phase $(Cr,Fe)_{23}C_6$ was also clearly established.

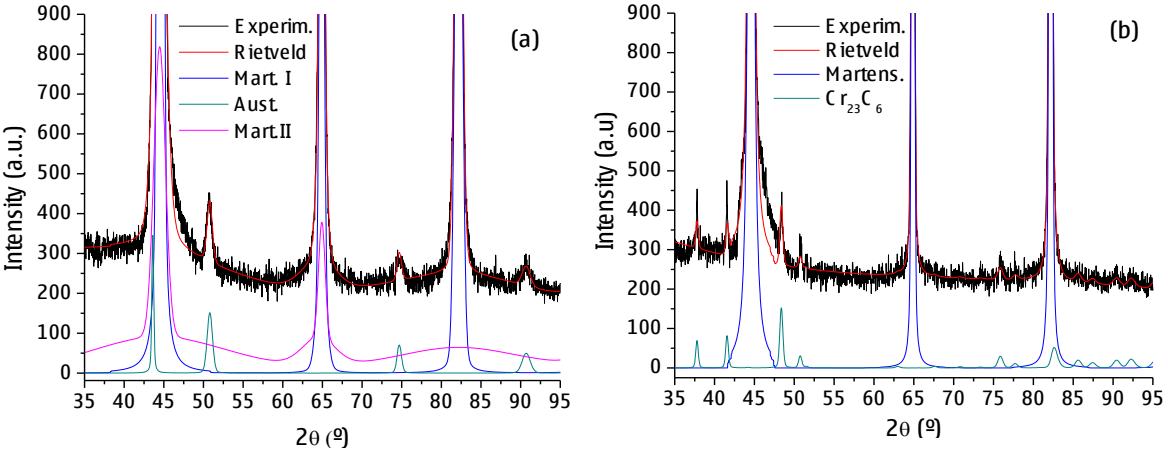

Fig. 7. XRD spectra of the AW (a) and PWHT-8h (b) samples.

The features of XRD spectra were consistent with the expected behavior of the material during welding and PWHT: as for the minor phases, a (low) fraction of retained austenite for the AW sample, which decomposes to martensite during the treatment, and presence of the most stable carbidic phase ($(Cr,Fe)_{23}C_6$) for the heat-treated samples. Other carbides or nitrides cannot be identified by XRD due to their very low volume fraction. On the other hand, the peaks of the matrix phase (martensite) were broader for the AW sample than for the PWHT sample. This fact indicates that in the multipass welding process, although overheating of some martensite regions coming from the first passes could operate as a kind of tempering (leading to a coarsening of the diffraction domains and hence to a narrowing of the diffraction peaks), the dominating effect is that of fresh martensite, i.e., a peak broadening due to the highly strained and small-sized martensite structure.

4. Conclusions

In this work the effect of PWHT's of varying duration on the hardness of a welded joint of a P91 steel were studied. The analysis of cross sections of the welds suggests the following conclusions:

- A narrow heat-affected zone (HAZ) 4 mm wide was detected, composed by a thin (~0.2 mm) coarse-grained layer with high hardness, a fine-grained region exhibiting grains up to 4 μm in size, and a soft intercritical region with low hardness, located 3 to 4 mm away from the fusion line.
- The results of hardness measurements suggest that a PWHT of 2h at 760 ºC is enough to reestablish the strength of the P91 steel after the welding process.

- XRD examination gave consistent indications of the microstructural changes occurred during multipass welding and PWHT.

Acknowledgements

This work has been done within the framework of the Scientific and Technical Cooperation Agreement between the Mincyt (Argentina) and Concytec (Perú) under the PE/01/11 contract. Special thanks are given to Eng. Walter Manrique and the technical staff of the Technological Welding Center – SOLDEXA (Lima, Perú) for preparing the welding joints. We are also indebted with Tec. Alicia Petragalli and Dr. Daniel Vega, from the XRD Laboratory, Condensed Matter Physics Department of the CNEA for X-ray diffraction measurements.

References

Aborn, R.H., 1956. Low Carbon Martensite. Transactions of American Society for Metals 48, 51-57.

Bell, K. Elevated Temperature Midlife Weldment Cracking. Report 597/1997. The Welding Institute, Abington, UK 1997.

Ellis, F.V., Viswanathan, R., 1998. Review of Type IV Cracking in Piping Welds. Integrity of High Temperature Welds. Professional Engineering Publishing Ltd; London, pp. 125.

Foldyna, V., Kubon, Z., Jakovoba, A., Vodarek, V., 1996. Proceedings 9th International Symposium on Creep Resistant Metallic Materials Hradecnad Moravicí, Vitkovice, Czech Republic, pp. 203.

Francis, J.A., Mazur, W., Bhadeshia, H.K.D.H., 2006. Type IV Cracking in Ferritic Power Plant Steels. Materials Science and Technology 22, 1387-1395.

Grong, O., 1994. "Metallurgical Modelling of Welding"; Institute of Materials, London.

Hasegawa, Y., Ohgami, M., Okumara, Y., 2001. Quantification of the Factors for Type IV Softening of Tungsten containing Creep Resistant Steel ASME Gr.92. In: Viswanathan, R., Bakker, W.T., Parker, J.D. (Eds.). Proceedings of Third Conference on Advances in Materials Technology for Fossil PowerPlants, The Institute of Metals; London, pp. 457.

Lutterotti, L., Matthies, S., Wenk, H.R., 1999. MAUD: A friendly Java Program for Material Analysis using Diffraction. IUCr: Newsletter of the CPD, 21, 14-15.

Moitra, A., Parameswaran, P.R., Sreenivasan, P.R., Mannan, S.L., 2002. A Toughness Study of the Weld Heat-Affected Zone of a 9Cr-1Mo Steel. Materials Characterization 48, 55-61.

Orr, J., Burton, D., 1992. In: J. Orr (Ed.) Proceedings "ECSC Information Day: Manufacture and Properties of Steel P91 for the Power Plant and Process Industries", Verein Deustscher Eisenhüttenleute, Düsseldorf, Germany.

Tamura, M., Ikeda, K., Esaka, H., Shinozuka, K., 2001. Precipitation Behavior of NbC in 9%Cr1%Mo0.2%VNb Steel. Iron and Steel Institute of Japan International 41, 908-914.

Viswanathan, R., 1989. Damage Mechanisms and Life Assessment of High Temperature Components, ASM International, Ohio.

Zavaleta Gutiérrez, N.E., Marrero, J., Danón, C.A., de Cicco, H., Luppo, M.I., 2011. Evolution of Precipitated Phases during Prolonged Tempering in a 9%Cr1%MoVNb Ferritic-Martensitic Steel: Influence on Creep Performance. Materials Science and Engineering A 528, 4019-4029.